

1     **The limited ability of posaconazole to cure both acute and chronic *Trypanosoma cruzi***  
2                                   **infections revealed by highly sensitive *in vivo* imaging**

3  
4  
5     Amanda Fortes Francisco,<sup>1</sup> Michael D. Lewis,<sup>1,4</sup> Shiromani Jayawardhana,<sup>1</sup> Martin C.  
6     Taylor,<sup>1</sup> Eric Chatelain<sup>2</sup> and John M. Kelly<sup>1,3</sup>

7  
8  
9  
10    <sup>1</sup>Department of Pathogen Molecular Biology  
11    London School of Hygiene and Tropical Medicine  
12    Keppel Street, London WC1E 7HT, UK.

13  
14    <sup>2</sup>Drugs for Neglected Diseases initiative (DNDi)  
15    15 Chemin Louis-Dunant, 1202 Geneva, Switzerland.

16  
17    <sup>3</sup>**Corresponding author:** Email: [john.kelly@lshtm.ac.uk](mailto:john.kelly@lshtm.ac.uk)

18  
19  
20    **Short running title:** Limited efficacy of posaconazole against Chagas disease.

21  
22  
23    <sup>4</sup>Current address: Laboratory of Parasitic Diseases, National Institute of Allergy and  
24    Infectious Diseases, Bethesda, MD 20892, USA.

25

26 **ABSTRACT**

27 The anti-fungal drug posaconazole has shown significant activity against *Trypanosoma cruzi*  
28 *in vitro* and in experimental murine models. Despite this, in a recent clinical trial it displayed  
29 limited curative potential. Drug testing is problematic in experimental Chagas disease  
30 because of difficulties in demonstrating sterile cure, particularly during the chronic stage of  
31 infection when parasite burden is extremely low and tissue distribution ill-defined. To better  
32 assess posaconazole efficacy against acute and chronic Chagas disease, we have exploited a  
33 highly sensitive bioluminescence imaging system which generates data with greater accuracy  
34 than other methods, including PCR-based approaches. Mice inoculated with bioluminescent  
35 *T. cruzi* were assessed by *in vivo* and *ex vivo* imaging, with cyclophosphamide-induced  
36 immunosuppression used to enhance the detection of relapse. Posaconazole was found to be  
37 significantly inferior to benznidazole as a treatment for both acute and chronic *T. cruzi*  
38 infections. Whereas 20 days treatment with benznidazole was 100% successful in achieving  
39 sterile cure, posaconazole failed in almost all cases. Treatment of chronic infections with  
40 posaconazole did however significantly reduce infection-induced splenomegaly, even in the  
41 absence of parasitological cure. The imaging-based screening system also revealed that  
42 adipose tissue is a major site of recrudescence in mice treated with posaconazole in the acute,  
43 but not the chronic stage of infection. This *in vivo* screening model for Chagas disease is  
44 predictive, reproducible and adaptable to diverse treatment schedules. It should provide  
45 greater assurance that drugs are not advanced prematurely into clinical trial.

46 .

47

48

49

50

51 **INTRODUCTION**

52 Chagas disease is a major public health problem in Latin America and is increasingly  
53 prevalent in other regions as a result of migration patterns (1-2). The causative agent,  
54 *Trypanosoma cruzi*, is transmitted to humans predominantly by hematophagous triatomine  
55 bugs, although other routes include contaminated food and drink, blood transfusion and  
56 congenital transmission. Following infection, patients progress to the acute stage of the  
57 disease, where parasites are readily detectable in the bloodstream by microscopic  
58 examination. In most individuals, immune-mediated responses suppress parasitemia within 4-  
59 6 weeks and the majority of patients then remain asymptomatic, despite a life-long low-level  
60 infection. However, years or often decades later, about 30% of those infected develop chronic  
61 Chagas disease pathology, typically cardiomyopathy and/or digestive megasyndromes (3).  
62 Because of the complex and long-term course of the infection, vaccine development is  
63 considered to be extremely challenging and most biomedical research has focussed on  
64 improving chemotherapy.

65

66 For the last 40 years, the nitroheterocyclic compounds benznidazole and nifurtimox have  
67 been the only drugs available to treat Chagas disease (4-5). This is despite the fact that  
68 therapeutic schedules are long, treatment failures have been frequently reported, and both  
69 drugs exhibit toxicity. In addition, their efficacy in preventing or alleviating chronic disease  
70 pathology remains to be conclusively demonstrated (6-7). Benznidazole and nifurtimox are  
71 prodrugs and both are activated within *T. cruzi* by the same mitochondrial nitroreductase  
72 (TcNTR) (8) leading to the generation of reactive metabolites which mediate parasite killing  
73 (9-11). This shared activation mechanism provides potential for cross-resistance (8, 12, 13)  
74 and highlights the need to identify additional therapeutic agents which target distinct  
75 biochemical pathways. In this context, sterol metabolism in *T. cruzi* has generated

76 considerable interest, particularly the enzymes involved in ergosterol biosynthesis (14, 15).  
77 The anti-fungal drug posaconazole for example, is a potent inhibitor of the *T. cruzi* sterol  
78 14 $\alpha$ -demethylase (CYP51) and has shown significant anti-parasitic activity *in vitro* and *in*  
79 *vivo* (16-18). Furthermore, combination therapy with benznidazole has demonstrated that  
80 murine infections can be cured with a reduced dosing regime (19, 20) However, in a recent  
81 randomised clinical trial against chronic *T. cruzi* infection, posaconazole was shown to have  
82 limited curative potential (21) and *in vitro* studies have found it to be less active than  
83 benznidazole (22).

84

85 The vast majority of Chagas disease patients are only diagnosed once they begin to display  
86 chronic disease pathology, or after testing prior to blood donation or surgical procedures.  
87 Drug trials against chronic stage infections are particularly challenging because it is difficult  
88 to unequivocally demonstrate sterile cure. In addition, lack of knowledge of the sites of  
89 parasite persistence can be a confounding factor that impacts on the reproducibility of PCR-  
90 based methodologies, making it difficult to accurately assess parasite burden in real time. To  
91 streamline the drug discovery process, we sought to improve the utility of current predictive  
92 models of experimental Chagas disease by developing an enhanced *in vivo* imaging system.  
93 This was achieved by engineering trypanosomes to express a red-shifted luciferase reporter  
94 which emits tissue-penetrating orange-red light ( $\lambda_{em}$  617 nm) (23, 24). In *T. cruzi*, the  
95 bioluminescent reporter is expressed at similar levels in different parasite life-cycle stages,  
96 has no effect on growth properties or virulence, and is maintained at constant levels for more  
97 than 12 months in the absence of selective drug pressure. Importantly, this *in vivo* imaging  
98 system has a limit of detection of between 100 and 1000 parasites, and has allowed parasite  
99 burden to be assessed in real time during experimental chronic infections in individual mice  
100 (24). Throughout chronic infections, dynamic bioluminescence foci can appear and disappear

101 over a period of less than 24 hours (24), consistent with a scenario where infected cells are  
102 being trafficked to and from peripheral sites. In BALB/c mice infected with the CL Brener  
103 strain, the gastrointestinal tract was found to be the major site of parasite persistence.  
104 Unexpectedly, in this model, infection of the heart was rarely observed in the chronic stage,  
105 even though these mice continued to exhibit cardiac inflammation and diffuse fibrosis,  
106 signatures of chronic Chagas disease pathology.

107

108 The enhanced sensitivity of this red-shifted luciferase based reporter system has the potential  
109 to provide new approaches for monitoring the effectiveness of drugs against experimental  
110 Chagas disease and should be a valuable addition to the drug discovery pipeline. Here, we  
111 describe its use to assess the efficacy of posaconazole to treat acute and chronic experimental  
112 infections. In line with a recent clinical trial, our predictive model suggests major limitations  
113 in the utility of this drug.

114

115

116

117

118

119

120

121

122

123

124

125 **MATERIALS AND METHODS**

126 **Mice and infections.** Female BALB/c mice were purchased from Charles River (UK) and  
127 CB17 SCID mice were bred in-house. Animals were maintained under specific pathogen-free  
128 conditions in individually ventilated cages, where they experienced a 12 hour light/dark cycle  
129 and had access to food and water *ad libitum*. All experiments were carried out under UK  
130 Home Office licence PPL 70/6997 and approved by the LSHTM Animal Welfare and Ethical  
131 Review Board. Mice were aged 8 – 12 weeks when infected with a bioluminescent reporter  
132 clone derived from the genome reference strain CL Brener (24). In standard experiments,  $1 \times 10^4$   
133 *in vitro* derived tissue-culture trypomastigotes (TCTs) or thawed cryopreserved  
134 bloodstream trypomastigotes (BTs) in 0.2 ml PBS were first used to infect SCID mice via  
135 intraperitoneal (i.p.) inoculation. Parasitaemic blood from these SCID mice was obtained 2 –  
136 3 weeks later and adjusted to  $5 \times 10^3$  BTs/ml with PBS. BALB/c mice were then infected  
137 with  $1 \times 10^3$  BTs via i.p injection (24).

138

139 **Treatment.** For drug treatment, benznidazole (Hoffmann-La Roche AG) was prepared from  
140 powder at 10 mg/ml in 7% Tween-80, 3% ethanol (v/v) and 90% (v/v) water. Posaconazole  
141 (Sequoia Research Products Ltd) was prepared at 2 mg/ml in 5% (v/v) dimethyl sulphoxide  
142 and 95% (v/v) HPMC-SV (0.5% (w/v) hydroxypropyl methylcellulose, 0.5% (v/v) benzyl  
143 alcohol and 0.4% (v/v) Tween 80). Noxafil (MSD Ltd.), a liquid formulation of posaconazole  
144 (40 mg/ml), was diluted to 2 mg/ml in water. Mice were treated with standard doses of  
145 benznidazole (100 mg/kg/day) or posaconazole (20 mg/kg/day) by oral gavage for  
146 consecutive days, as required. To facilitate detection of residual infection after treatment, in  
147 some experiments BALB/c mice were immunosuppressed with cyclophosphamide (200  
148 mg/kg) by i.p. injection at 3 – 4 day intervals, for a maximum of 3 doses.

149

150 ***In vivo* bioluminescence imaging.** Mice were injected i.p. with 150 mg/kg d-luciferin  
151 (Perkin-Elmer) in Dulbecco's Ca<sup>2+</sup>/Mg<sup>2+</sup> free PBS, then anaesthetized using 2.5% (v/v)  
152 gaseous isoflurane in oxygen. To measure bioluminescence, mice were placed in an IVIS  
153 Lumina II system (Caliper Life Science) and both dorsal and ventral images were acquired 10  
154 – 20 minutes after d-luciferin administration using LivingImage 4.3. Exposure times varied  
155 between 30 seconds and 5 minutes, depending on signal intensity. Anaesthesia was  
156 maintained throughout via individual nose-cones. After imaging was complete, mice were  
157 revived and returned to cages. To estimate parasite burden, whole body regions of interest  
158 (ROIs) were drawn using LivingImage v.4.3 to quantify bioluminescence expressed as total  
159 flux (photons/second; p/s). The detection threshold was established previously using data  
160 from control uninfected mice (24). Animals where bioluminescence intensity was  
161 consistently below  $5 \times 10^3$  p/s/sr/cm<sup>2</sup> in both dorsal and ventral images following  
162 immunosuppression, were regarded as cured, subject to confirmation by *ex vivo* assessment  
163 (below).

164

165 **Assessment of treatment efficacy by *ex vivo* imaging.** Selected organs and tissue samples  
166 from all mice were assessed for infection by *ex vivo* imaging (Figure 1e), as described  
167 previously (24). Briefly, mice were injected with 150 mg/kg d-luciferin i.p., then sacrificed  
168 by ex-sanguination under terminal anaesthesia 7 minutes later. Mice were perfused with 10  
169 ml 0.3 mg/ml d-luciferin in PBS via the heart. Organs and tissues were excised, transferred to  
170 a Petri dish or culture dish, soaked in 0.3 mg/ml d-luciferin in PBS, and then imaged as per  
171 live mice. Routinely, the rest of the carcass was also assessed for bioluminescence associated  
172 with skin, skeletal muscle or remaining adipose tissue. As with *in vivo* imaging,  
173 bioluminescence intensity of  $5 \times 10^3$  p/s/sr/cm<sup>2</sup> was used as the threshold to designate cure.

174

175 **PCR-based detection.** Heart, large intestine and blood tissues were snap frozen on dry ice  
176 and stored at  $-80^{\circ}\text{C}$  until required for DNA extraction. In the case of the gut, three one  
177 centimetre sections were pooled from the proximal colon, the mid-colon region and the  
178 rectum of each mouse. Samples were then thawed and immediately homogenized in at least  
179 200  $\mu\text{l}$  lysis buffer (4 M urea, 200 mM Tris, 20 mM NaCl, 200 mM EDTA, pH 7.4) per 50  
180 mg of tissue, using a BulletBlender Storm instrument (Next Advance). Proteinase K (Sigma)  
181 was added to the tissue suspension at 0.6 mg per 200  $\mu\text{l}$  and incubated at  $56^{\circ}\text{C}$  for 1 hour,  
182 then at  $37^{\circ}\text{C}$  overnight. DNA was extracted from lysates using a HighPure PCR template  
183 preparation kit (Roche), according to the manufacturer's instructions. Real-time PCR  
184 reactions were prepared using the QuantiTect SYBR Green PCR Kit (Qiagen) and run on a  
185 RotorGene 3000 instrument. Each reaction contained 50 ng DNA and 0.5  $\mu\text{M}$  of each primer.  
186 *T. cruzi*-specific primers TCZ-F/TCZ-R (25) targeted at the 195 bp satellite repeat ( $10^4$  copies  
187 in the CL Brener genome), or mouse-specific primers GAPDHf/GAPDHr (26) targeted at the  
188 murine *gapdh* gene, were used.

189

190 *T. cruzi*-specific qPCR Ct values were converted to inferred numbers of parasite equivalents  
191 (p.e.) by reference to a standard curve with a range of  $2.5 \times 10^6 - 2.5 \times 10^{-1}$  p.e./ml of tissue  
192 lysate. The *T. cruzi* standard curve was established from serial dilution of a DNA sample  
193 derived from 75 mg homogenised muscle tissue, spiked with  $2 \times 10^7$  epimastigotes, using  
194 DNA from unspiked equivalent samples as the diluent. Murine DNA content was determined  
195 by normalizing mouse-specific qPCR Ct values by reference to a standard curve with a range  
196 of  $2.5 \times 10^1 - 2.5 \times 10^{-4}$   $\mu\text{g}/\text{ml}$ . The murine standard curve was established from serial  
197 dilution of a mouse DNA sample using herring sperm DNA as the diluent. Due to the non-  
198 specific fluorescence inherent to this SYBR green qPCR method, we defined parasite  
199 detection limits as the mean +3SDs for samples from uninfected control mice.

200

201 **Statistics.** Results are shown as mean  $\pm$ SD or SEM where sample sizes are equal or non-  
202 equal, respectively. Individual animals were used as the unit of analysis for *in vivo* and *ex*  
203 *vivo* experiments. For spleen mass, means were compared using Student's *t*-test.

204

205

206

207

208

209

210

211

212

213

214

215

216

217

218

219

220

221

222

223 **RESULTS**

224 **Benznidazole and posaconazole efficacy against chronic stage *T. cruzi* infections.**

225 BALB/c mice, infected i.p. with  $10^3$  bioluminescent bloodstream form *T. cruzi*  
226 trypomastigotes (CL Brener strain), were monitored by *in vivo* imaging (Fig. 1A, Materials  
227 and Methods). In this experimental model, peak parasitemia occurs after 14 days, and is  
228 followed by an immune-mediated reduction in parasite load during progress to the chronic  
229 stage, 40-50 days post-infection (dpi) (Fig. 2B) (24). After 74 days, cohorts of mice were  
230 treated daily for 20 days by the oral route with benznidazole (100 mg/kg), or with one of two  
231 posaconazole formulations (20 mg/kg). These dosing regimes have been widely used for  
232 experimental purposes (19, 20, 27, 28). Benznidazole acted rapidly and the whole body  
233 bioluminescence of each mouse fell to undetectable levels within 5 days (Fig. 1B and 2A).  
234 Posaconazole was slower acting, but by the conclusion of the treatment period, the inferred  
235 parasite load had also dropped to background levels. The bioluminescence profile during  
236 treatment was very similar with both posaconazole formulations (Fig. 1C and D, and 2A). 20  
237 days after the cessation of treatment (113 dpi), half the mice in each cohort were  
238 immunosuppressed (Materials and Methods). No signs of infection were observed in any of  
239 the benznidazole treated mice in either the immunosuppressed or immunocompetent groups  
240 (Fig. 1B). However, in the posaconazole treated group, the infection relapsed in all of the  
241 cyclophosphamide treated mice (Fig. 1C and D, and 2a; Table 1).

242

243 Organs from all of the mice were assessed for infection by *ex vivo* imaging at the  
244 experimental end-point (Fig. 1e, Materials and Methods). In accordance with experiments  
245 using this and other mouse-parasite combinations (24; M.L., unpublished observations),  
246 persistent bioluminescent foci at this point of the infection (~148 dpi) were associated  
247 predominantly with the gastrointestinal tract (mainly the colon and stomach) in untreated

248 mice, and only sporadically with other major organs/tissues. Mice were designated as cured,  
249 if they were bioluminescence negative by both *in vivo* and *ex vivo* imaging, following  
250 cyclophosphamide treatment (Materials and Methods). Based on these criteria, none of the  
251 nine chronically infected mice treated with posaconazole and subsequently  
252 immunosuppressed were cured. In contrast, all five mice that were treated with benznidazole  
253 and then immunosuppressed were inferred to be parasite-free.

254

255 Quantitative PCR (qPCR) after immunosuppression has until now been the most accurate  
256 technique for defining parasitological cure in *T. cruzi* infections (20, 28, 29). However, when  
257 we assessed the efficacy of this method in our chronic infection model, we found that PCR  
258 methodology had a tendency to overestimate cure-rate, particularly with posaconazole  
259 treatment. In chronically infected untreated mice, pooled gut tissue (Materials and Methods)  
260 was PCR-positive in each case, and negative when mice were treated with benznidazole for  
261 20 days, including the group that was subsequently immunosuppressed (Fig. 3A). With the  
262 posaconazole treated non-immunosuppressed mice, gut tissue was PCR-negative in 9 out of 10  
263 cases, also consistent with a high rate of cure. This inferred cure rate was reduced when tissue  
264 derived from mice that had also been cyclophosphamide treated was analysed. The number of  
265 PCR-negative (cured) animals fell to 4 out of 9, indicating that some low level infections only  
266 become detectable by PCR after immunosuppression. However, even this reduced cure rate is  
267 at odds with data from bioluminescence imaging, which demonstrated unequivocally that  
268 posaconazole failed to eradicate parasites in any of the treated mice (Fig. 1, Table 1). In the  
269 case of cardiac tissue, with one exception, results were PCR-negative in all cases (Fig. 3B), in  
270 accordance with bioluminescence imaging of chronic stage infections (Fig. 1, ref. 25). When  
271 blood samples were analysed, they were predominantly negative, even when mice were non-  
272 treated (Fig. 3c). Collectively, these results highlight the limitations of using PCR-based

273 approaches to define parasitological cure in this dynamic chronic stage model. The low level  
274 and sporadic nature of bloodstream parasitemia and the focal and highly dynamic nature of  
275 tissue infection, even within the gastro-intestinal tract, appear to be the confounding factors  
276 which result in an overestimation of the cure-rate when determined by qPCR alone.

277

278 To further assess the ability of benznidazole to cure chronically infected mice, we reduced  
279 the treatment period to 10 and 5 oral doses (100 mg/kg/day) over consecutive days. In each  
280 case, bioluminescence fell below the level of detection by the completion of treatment, and  
281 subsequent immunosuppression of these mice did not lead to a relapse, as assessed by either  
282 *in vivo* and *ex vivo* imaging (Fig. 4). In this experimental model therefore, there is scope to  
283 reduce the length of benznidazole treatment of chronic *T. cruzi* infections and still achieve a  
284 curative outcome.

285

286 Splenomegaly is frequently observed in experimental *T. cruzi* infections, both acute and  
287 chronic. Here, we observed that the spleens of chronically infected mice were approximately  
288 twice the mass of those from non-infected mice (Fig. 5). This spleen enlargement could be  
289 reversed by curative treatment with benznidazole (assessed by *in vivo* and *ex vivo* imaging,  
290 with an immunosuppressed group in parallel, Fig. 1). Interestingly, there was also a reversal  
291 of splenomegaly following posaconazole treatment. In these mice, there was a major  
292 reduction in parasite burden, but a curative outcome was not achieved (Fig. 1). Therefore,  
293 splenomegaly in this model is linked with parasite load and can be largely reversed, at least in  
294 the short term, without having to achieve a sterile cure.

295

296 **Benznidazole and posaconazole efficacy against acute stage *T. cruzi* infections.** Using the  
297 same experimental model as above, we compared the ability of benznidazole and

298 posaconazole to cure acute stage *T. cruzi* infections. Treatment was started at the peak of  
299 parasite burden (14 dpi) with standard oral doses (benznidazole, 100 mg/kg; posaconazole, 20  
300 mg/kg) administered daily for 20 days. Similar to the chronic stage infections, benznidazole  
301 treatment resulted in a rapid fall in parasite load, with bioluminescence reduced to  
302 background levels within 5 days (Fig. 2B and 6B). There was no relapse of infection, when  
303 mice were assessed by *in vivo* or *ex vivo* imaging following immunosuppression (Fig. 6B and  
304 E), and all mice treated with benznidazole were therefore designated as cured.

305

306 With posaconazole treatment, the reduction in bioluminescence was much more rapid than  
307 had been observed with chronic stage infections (compare Fig. 2A and B), and only  
308 marginally slower than with benznidazole. Again, there were no significant differences in the  
309 efficacy of the two posaconazole formulations. Bioluminescence remained close to, or only  
310 slightly above background levels, until the mice were treated with cyclophosphamide  
311 (initiated 49 dpi) (Fig. 2B and 6). At this point, there was a rapid rebound in parasite load in  
312 most cases, with 16 out of 19 mice displaying a clear bioluminescence signal (Fig. 6, Table  
313 1). Of the three mice judged to be cured, one had been treated with the Noxafil and two with  
314 the HPMC-SV posaconazole formulation (Materials and Methods). These results therefore  
315 suggest that although posaconazole is more effective at reducing the parasite load during the  
316 acute stage than it is during the chronic stage, it has only a limited ability to achieve a sterile  
317 cure in this experimental model, in either stage of the disease.

318

319 In 9 out of the 16 posaconazole treated mice which relapsed after cyclophosphamide  
320 treatment, we observed that adipose tissue was the major site of recrudescence (Fig. 7A, as  
321 example). This suggests that the ability of parasites to persist in this location following acute  
322 stage posaconazole treatment is a common phenomenon. In contrast ( $P<0.05$ ), when mice in

323 the chronic stage of infection were treated and then immunosuppressed, only 1 out of 9  
324 animals displayed a significant parasite burden in this tissue (shown Fig. 1E (iv)), with the  
325 gastro-intestinal tract being the major site of parasite recrudescence (Fig. 7B).

326

327

328

329

330

331

332

333

334

335

336

337

338

339

340

341

342

343

344

345 **DISCUSSION**

346 Progress in developing new drugs for chronic *T. cruzi* infections has been limited by  
347 difficulties in unambiguously demonstrating parasitological cure. An underlying cause, as  
348 inferred from murine infections, could be the discrete nature of infection foci during chronic  
349 Chagas disease, and their highly dynamic spatiotemporal distribution (24). As a consequence,  
350 there is a risk of overestimating cure rates associated with unguided tissue sampling, even  
351 when using PCR-based technology. Highly sensitive bioluminescence imaging circumvents  
352 some of these issues by facilitating the real time evaluation of parasite burden throughout  
353 long term infections, with minimal tissue sampling bias.

354

355 Several studies have reported on the efficacy of the CYP51 inhibitor posaconazole, and its  
356 ability to cure *T. cruzi* infections in murine models (17-20). Despite this, when the drug was  
357 advanced into clinical trials, it failed to provide significant benefit to chronically infected  
358 patients, in terms of parasitological cure (21). In line with this, data from our predictive  
359 model imply that posaconazole has limited potential against both stages of Chagas disease  
360 (Table 1). *In vivo* imaging revealed that although posaconazole is highly effective at reducing  
361 parasite burden, it does not readily cure acute or chronic *T. cruzi* infections. When mice in the  
362 acute stage were treated, the bioluminescence-inferred parasite burden was reduced by more  
363 than 3 orders of magnitude within 7 days, however sterile cure was rarely achieved (Fig. 2  
364 and 6). With chronic infections, posaconazole failed to cure any of the mice and the reduction  
365 in parasite load occurred more slowly (Fig. 1 and 2). This inability, in the vast majority of  
366 cases, to eradicate parasites has parallels with *in vitro* studies. These showed that although the  
367  $EC_{50}$  of posaconazole against intracellular *T. cruzi* is in the nanomolar range, it often fails to  
368 eliminate parasite infection (22). One reason for the faster rate of parasite knockdown in the  
369 acute stage (Fig. 2) might be that parasites replicate more rapidly, and are therefore more

370 susceptible to drugs that perturb lipid metabolism. Alternatively, in the chronic stage, when  
371 parasites are restricted predominantly to gastro-intestinal sites (24), they may be less  
372 accessible compared to the acute stage, when parasites can be targeted in all organs, although  
373 this explanation is less likely given the pharmacokinetic and distribution properties of  
374 posaconazole (30).

375

376 Typically, treatment with posaconazole reduced whole body bioluminescence to background  
377 levels, with few infection foci detectable in the absence of immunosuppression. Given the  
378 sensitivity of the imaging procedure (24), this suggests that the remaining parasites survive in  
379 low numbers within small groups of infected cells. As a result, detection of residual parasites  
380 by PCR-based methods is problematic (Fig. 3). In the past, this may have led to an over-  
381 estimation of the ability of posaconazole to cure chronic infections. Posaconazole treatment  
382 has been shown to reverse spleen enlargement, a characteristic of murine *T. cruzi* infections.  
383 In these experiments, curative outcome was inferred on the basis of several criteria (27).  
384 However, here we demonstrate that reversal of splenomegaly is not indicative of sterile cure  
385 (Fig. 5), but is linked merely with a reduction in parasite burden.

386

387 In more than 50% of cases (9/16), end-point *ex vivo* analysis of acute stage infections  
388 identified visceral fat as the tissue with the highest parasite burden following relapse (Fig. 7).  
389 There are several reasons why posaconazole could be less effective at eliminating parasites  
390 from this site. Parasite load may be higher in adipose tissues (24), differential drug  
391 accessibility may be an issue, or parasites could be less susceptible in a lipid/sterol rich  
392 environment. When mice treated during the chronic stage were examined after relapse, only 1  
393 mouse out of 9 displayed a detectable level of bioluminescence in visceral fat (Fig. 7). At this  
394 stage of an infection, parasites are restricted mainly to the gastro-intestinal tract, and only

395 sporadically detected in the visceral fat, or other tissues, by bioluminescence. In chronic  
396 infections therefore, this tissue is less likely to be relevant as a reservoir for parasite survival  
397 following drug treatment. Previous studies have identified parasites localised in adipose  
398 tissue in some chronic human infections (31, 32) In non-treated mice however,  
399 bioluminescence imaging did not identify the visceral fat as a primary site of recrudescence  
400 during a chronic infection (see Fig. 7).

401

402 In summary, we have shown that benznidazole is significantly more effective at curing both  
403 acute and chronic *T. cruzi* infections than posaconazole. The utility and flexibility of the *in*  
404 *vivo* imaging procedure we have developed has potential for making a valuable contribution  
405 to the Chagas disease drug discovery pipeline. It can also, as shown here, add value to the  
406 screening process by providing new information on drug efficacy. Importantly, the  
407 availability of such a sensitive *in vivo* technique should provide greater assurance that drugs  
408 are not advanced prematurely into clinical trial.

409

410

411

412

413

414

415

416

417

418

419 **ACKNOWLEDGEMENTS**

420 This work was supported by the Drugs for Neglected Diseases initiative (DNDi) and grants  
421 from the Wellcome Trust (Grant 084175) and the British Heart Foundation (Grant  
422 PG/13/88/30556). For the work described in this manuscript, DNDi received financial  
423 support from the Directorate-General for International Cooperation (DGIS), The Netherlands.

424

425 We thank Bruce Branchini for the *PpyRE9H* luciferase gene, and Michael Miles, Karin  
426 Seifert, Stéphanie Braillard and members of the DNDi Australian LO Consortium for  
427 valuable discussion.

428

429

430

431

432

433

434

435

436

437

438

439

440

441

442 **REFERENCES**

- 443 1. **Moncayo A, Silveira AC.** 2009. Current epidemiological trends for Chagas disease in  
444 Latin America and future challenges in epidemiology, surveillance and health policy.  
445 *Mem Inst Oswaldo Cruz* **104**:17-30.
- 446 2. **Rassi A Jr, Rassi A, Marin-Neto JA.** 2010. Chagas disease. *Lancet* **375**:1388-1402.
- 447 3. **Marin-Neto JA, Rassi A Jr, Morillo CA, Avezum A, Connolly SJ, Sosa-Estani S,**  
448 **Rosas F, Yusuf S.** 2008. Rationale and design of a randomized placebo-controlled  
449 trial assessing the effects of etiologic treatment in Chagas' cardiomyopathy: The  
450 BENznidazole Evaluation For Interrupting Trypanosomiasis (BENEFIT). *Am Heart J*  
451 **156**:37-43.
- 452 4. **Wilkinson SR, Kelly JM.** 2009. Trypanocidal drugs: mechanisms, resistance and  
453 new targets. *Expert Rev Molec Med* **11**:e31.
- 454 5. **Patterson S, Wyllie S.** 2014. Nitro drugs for the treatment of trypanosomatids  
455 diseases: past, present, and future prospects. *Trends Parasitol* **30**:289-298.
- 456 6. **Castro JA, de Mecca MM, Bartel LC.** 2006. Toxic side effects of drugs used to  
457 treat Chagas disease (American trypanosomiasis). *Hum Exp Toxicol* **25**:471-479.
- 458 7. **Le Loup G, Pialoux G, Lescure FX.** 2011. Update in treatment of Chagas disease.  
459 *Curr Opin Infect Dis* **24**:428-434.
- 460 8. **Wilkinson SR, Taylor MC, Horn D, Kelly JM, Cheeseman I.** 2008. A mechanism  
461 for cross-resistance to nifurtimox and benznidazole in trypanosomes. *Proc Natl Acad*  
462 *Sci USA* **105**:5022-5027.
- 463 9. **Hall BS, Wilkinson SR.** 2012. Activation of benznidazole by trypanosomal type I  
464 nitroreductases results in glyoxal formation. *Antimicrob Agents Chemother* **56**:115-  
465 123.

- 466 10. **Hall BS, Bot C, Wilkinson SR.** 2011. Nifurtimox activation by trypanosomal type I  
467 nitroreductases generates cytotoxic nitrile metabolites. *J Biol Chem* **286**:13088-  
468 13095.
- 469 11. **Trochine A, Creek DJ, Faral-Tello P, Barrett MP, Robello C.** 2014. Benznidazole  
470 biotransformation and multiple targets in *Trypanosoma cruzi* revealed by  
471 metabolomics. *PLoS Negl Trop Dis* **8**:e2844.
- 472 12. **Mejia AM, Hall BS, Taylor MC, Gómez-Palacio A, Wilkinson SR, Triana-  
473 Chávez O, Kelly JM.** 2012. Benznidazole-resistance in *Trypanosoma cruzi* is a  
474 readily acquired trait that can arise independently in a single population. *J Inf Dis*  
475 **206**:220-228.
- 476 13. **Campos MCO, Leon LL, Taylor MC, Kelly JM.** 2014. Benznidazole-resistance in  
477 *Trypanosoma cruzi*: evidence that distinct mechanisms can act in concert. *Mol*  
478 *Biochem Parasitol* **193**:17-19.
- 479 14. **Urbina JA.** 2009. Ergosterol biosynthesis and drug development for Chagas disease.  
480 *Mem Inst Oswaldo Cruz* **104** Suppl 1:311-318.
- 481 15. **Lepesheva GI, Villalta F, Waterman MR.** 2012. Targeting *Trypanosoma cruzi*  
482 sterol 14 $\alpha$ -demethylase (CYP51). *Adv Parasitol* **75**:65-87.
- 483 16. **Pinazo MJ, Espinosa G, Gállego M, López-Chejade PL, Urbina JA, Gascón J.**  
484 2010. Successful treatment with posaconazole of a patient with chronic Chagas  
485 disease and systemic lupus erythematosus. *Am J Trop Med Hyg* **82**:583-587.
- 486 17. **Lepesheva GI, Hargrove TY, Anderson S, Kleshchenko Y, Furtak V, Wawrzak  
487 Z, Villalta F, Waterman MR.** 2010. Structural insights into inhibition of sterol  
488 14 $\alpha$ -demethylase in the human pathogen *Trypanosoma cruzi*. *J Biol Chem*  
489 **285**:25582-25590.

- 490 18. **Urbina JA, Payares G, Contreras LM, Liendo A, Sanoja C, Molina J, Piras M,**  
491 **Piras R, Perez N, Wincker P, Loebenberg D.** 1998. Antiproliferative effects and  
492 mechanism of action of SCH 56592 against *Trypanosoma (Schizotrypanum) cruzi*:  
493 *in vitro* and *in vivo* studies. *Antimicrob Agents Chemother* **42**:1771-1777.
- 494 19. **Diniz L de F, Urbina JA, de Andrade IM, Mazzeti AL, Martins TA, Caldas IS,**  
495 **Talvani A, Ribeiro I, Bahia MT.** 2013. Benznidazole and posaconazole in  
496 experimental Chagas disease: positive interaction in concomitant and sequential  
497 treatments. *PLoS Negl Trop Dis* **7**:e2367.
- 498 20. **Bustamante JM, Craft JM, Crowe BD, Ketchie SA, Tarleton RL.** 2014. New,  
499 combined, and reduced dosing treatment protocols cure *Trypanosoma cruzi* infection  
500 in mice. *J Infect Dis* **209**:150-162.
- 501 21. **Molina I, Gómez i Prat J, Salvador F, Treviño B, Sulleiro E, Serre N, Pou D,**  
502 **Roure S, Cabezos J, Valerio L, Blanco-Grau A, Sánchez-Montalvá A, Vidal X,**  
503 **Pahissa A.** 2014. Randomized trial of posaconazole and benznidazole for chronic  
504 Chagas' disease. *N Engl J Med* **370**:1899-1908.
- 505 22. **Moraes CB, Giardini MA, Kim H, Franco CH, Araujo-Junior AM, Schenkman**  
506 **S, Chatelain E, Freitas-Junior LH.** 2014. Nitroheterocyclic compounds are more  
507 efficacious than CYP51 inhibitors against *Trypanosoma cruzi*: implications for  
508 Chagas disease drug discovery and development. *Sci Rep* **4**:4703.
- 509 23. **Branchini BR, Ablamsky DM, Davis AL, Southworth TL, Butler B, Fan F,**  
510 **Jathoul AP, Pule MA.** 2010. Red-emitting luciferases for bioluminescence reporter  
511 and imaging applications. *Anal Biochem* **396**:290-297.
- 512 24. **Lewis MD, Fortes Francisco A, Taylor MC, Burrell-Saward H, McLatchie AP,**  
513 **Miles MA, Kelly JM.** 2014. Bioluminescence imaging of chronic *Trypanosoma cruzi*

- 514 infections reveals tissue-specific parasite dynamics and heart disease in the absence of  
515 locally persistent infection. *Cell Microbiol* **16**:1285-1300.
- 516 25. **Cummings KL, Tarleton RL.** 2003. Rapid quantitation of *Trypanosoma cruzi* in  
517 host tissue by real-time PCR. *Mol Biochem Parasitol* **129**:53-59.
- 518 26. **Cencig S, Coltel N, Truyens C, Carlier Y.** 2011. Parasitic loads in tissues of mice  
519 infected with *Trypanosoma cruzi* and treated with AmBisome. *PLoS Negl Trop Dis*  
520 **5**:e1216.
- 521 27. **Olivieri BP, Molina JT, de Castro SL, Pereira MC, Calvet CM, Urbina JA,**  
522 **Araújo-Jorge TC.** 2010. A comparative study of posaconazole and benznidazole in  
523 the prevention of heart damage and promotion of trypanocidal immune response in a  
524 murine model of Chagas disease. *Int J Antimicrob Agents* **36**:79-83.
- 525 28. **Cencig S, Coltel N, Truyens C, Carlier Y.** 2012. Evaluation of benznidazole  
526 treatment combined with nifurtimox, posaconazole or AmBisome® in mice infected  
527 with *Trypanosoma cruzi* strains. *Int J Antimicrob Agents* **40**:527-532.
- 528 29. **Dos Santos FM, Caldas S, de Assis Cáu SB, Crepalde GP, de Lana M, Machado-**  
529 **Coelho GL, Veloso VM, Bahia MT.** 2008. *Trypanosoma cruzi*: Induction of  
530 benznidazole resistance in vivo and its modulation by in vitro culturing and mice  
531 infection. *Exp Parasitol* **120**:385-390.
- 532 30. **Li Y, Theuretzbacher U, Clancy CJ, Nguyen MH, Derendorf H.** 2010.  
533 Pharmacokinetic/pharmacodynamic profile of posaconazole. *Clin Pharmacokinet*  
534 **49**:379-396.
- 535 31. **Ferreira AV, Segatto M, Menezes Z, Macedo AM, Gelape C, de Oliveira**  
536 **Andrade L, Nagajyothi F, Scherer PE, Teixeira MM, Tanowitz HB.** 2011.  
537 Evidence for *Trypanosoma cruzi* in adipose tissue in human chronic Chagas disease.  
538 *Microbes Infect* **13**:1002-1005.

- 539 32. **Nagajyothi F, Machado FS, Burleigh BA, Jelicks LA, Scherer PE, Mukherjee S,**  
540 **Lisanti MP, Weiss LM, Garg NJ, Tanowitz HB.** 2012. Mechanisms of  
541 *Trypanosoma cruzi* persistence in Chagas disease. *Cell Microbiol* **14**:634-643.  
542  
543  
544  
545  
546  
547  
548  
549  
550  
551  
552  
553  
554  
555  
556  
557  
558  
559  
560  
561  
562

563 **FIG 1.** Benznidazole, but not posaconazole, cures mice chronically infected with  
564 *Trypanosoma cruzi*. Mice infected with bioluminescent *T. cruzi* were injected with 150  
565 mg/kg d-luciferin, anaesthetised and imaged using an IVIS Lumina II system (Materials and  
566 Methods). (a-d) Ventral (V) and dorsal (D) images of individual representative infected mice.  
567 (A) Non-treated mouse. (B) Mouse treated with 100 mg/kg benznidazole on days 74 – 93  
568 post-infection, then immunosuppressed by 200 mg/kg cyclophosphamide treatment on days  
569 113, 118 and 128. (C) Mouse treated with 20 mg/kg posaconazole (Noxafil formulation) on  
570 days 74 - 93, and then immunosuppressed, as above. (D) Mouse treated with posaconazole  
571 (HPMC-SV formulation) on days 74 - 93, and immunosuppressed, as above. (E) Tissue-  
572 specific *ex vivo* imaging. (i) Non-treated mouse 132 days post-infection (dpi). (ii) Mouse 147  
573 dpi, which had been treated with benznidazole, and then immunosuppressed, as described  
574 above. (iii and iv) Mice 147/148 dpi, which had been treated with posaconazole (Noxafil and  
575 HPMC-SV formulations respectively), then immunosuppressed, as above. (v) Schematic  
576 which identifies the positions of organs displayed in insets (i-iv). (Gut Mes, gut mesentery  
577 tissue; OES, oesophagus; SKM, skeletal muscle; STM, stomach; VIS FAT, visceral  
578 fat/adipose tissue). The heat-map is on a log<sub>10</sub> scale and indicates intensity of  
579 bioluminescence from low (blue) to high (red); the minimum and maximum radiances for the  
580 pseudocolour scale are shown.

581

582

583

584

585

586

587

588 **FIG 2.** Quantification of whole animal bioluminescence (ventral and dorsal) following  
589 treatment with benznidazole and posaconazole. (A) Infected mice treated starting 74 dpi for  
590 20 days by the oral route. (B) Mice treated starting 14 dpi for 20 days by the oral route. Red  
591 squares, untreated mice; n=5, acute; n=6 chronic. Blue squares, treated with benznidazole at  
592 100 mg/kg; n=10. Green squares, treated with posaconazole (Noxafil) at 20 mg/kg; n=9.  
593 Purple squares, treated with posaconazole (HPMC-SV formulation) at 20 mg/kg; n=10.  
594 Arrows indicate the start and end points of treatment. Grey lines indicate detection threshold  
595 determined as the mean (solid line) and mean +2SD (dashed line) of background  
596 bioluminescence of control uninfected mice. Crosses signify dates of cyclophosphamide  
597 treatment (200 mg/kg). Inoculation failed to result in an infection in one mouse in each of the  
598 acute and chronic infection studies. These mice were not treated (Noxafil cohort) and  
599 excluded from the analysis.

600

601

602

603

604

605

606

607

608

609

610

611

612

613 **FIG 3.** qPCR-inferred parasite loads in drug-treated chronically infected mice. DNA was  
614 extracted from large intestine (A), heart (B) and blood (C) samples and the relative amounts  
615 of *T. cruzi* and murine DNA were quantified by real-time PCR amplification of the multi-  
616 copy 195 bp satellite repeat and of the *gapdh* gene, respectively (Materials and Methods).  
617 The limit of detection is represented by the dotted line which corresponds to the mean +3SDs  
618 of large intestine, heart or blood samples from uninfected cells. Above this line, there is a  
619 linear correlation with parasite number as established by a standard curve (Materials and  
620 Methods). In (A) and (B), the base-line is equivalent to <1 parasite per 5 million murine  
621 cells). In (C), the base-line established with the multi-copy 195 bp repeat corresponds to 1  
622 parasite equivalent per  $\mu\text{l}$  blood. NI: non-infected; INT: infected non-treated; IBZ: infected,  
623 benznidazole treated (as in Fig. 1); IBZ, CYP: infected, benznidazole treated, then  
624 immunosuppressed with cyclophosphamide; IP1: infected, posaconazole (Noxafil) treated;  
625 IP1, CYP: infected, posaconazole (Noxafil) treated, then immunosuppressed with  
626 cyclophosphamide; IP2: infected, posaconazole (HPMC-SV formulation) treated; IP2, CYP:  
627 infected, posaconazole (HPMC-SV formulation) treated, then immunosuppressed.

628

629

630

631

632

633

634

635

636

637

638 **FIG 4.** Assessing the ability of benznidazole to cure mice chronically infected with  
639 *Trypanosoma cruzi* using 5 and 10 day treatment regimes. (A) Outline of experimental  
640 protocol. Cohorts of 6 mice were infected with bioluminescent *T. cruzi* (Materials and  
641 Methods). 103 days post-infection (dpi), they were treated with benznidazole (daily by the  
642 oral route, 100 mg/kg) for 5 days or 10 days. As indicated, mice were subsequently  
643 immunosuppressed with 3 i.p. doses of cyclophosphamide (200 mg/kg). (B) Ventral images  
644 of 3 representative mice from each cohort taken at the indicated dpi. (C) Representative *ex*  
645 *vivo* imaging of organs from infected mice 140 dpi (Materials and Methods). Organs are  
646 displayed in accordance with schematic in Fig. 1E (v). Heat-maps indicate intensity of  
647 bioluminescence from low (blue) to high (red) (log<sub>10</sub> scales); the minimum and maximum  
648 radiances for the pseudocolour scale are shown

649

650

651

652

653

654

655

656

657

658

659

660

661

662

663 **FIG 5.** Effect of chronic *Trypanosoma cruzi* infection and drug treatment on spleen mass. 74  
664 days post-infection, mice were treated with benznidazole (100 mg/kg) (IBZ) or posaconazole  
665 (20 mg/kg) (IP1, IP2; Noxafil and HPMC-SV formulations, respectively) by the oral route,  
666 daily for 20 days (see also Fig. 1). Spleens were harvested and weighed at the end of the  
667 experiment. Spleen weights in infected, non-treated mice (INT) were significantly greater  
668 than those in non-infected mice (NI) ( $P<0.0001$ ), or infected mice which had been treated  
669 ( $P<0.005$ , in each case).

670

671

672

673

674

675

676

677

678

679

680

681

682

683

684

685

686

687

688 **FIG 6.** Posaconazole has limited efficacy as a treatment for acute *Trypanosoma cruzi*  
689 infections. Mice (n = 10) were infected with bioluminescent *T. cruzi* (Fig. 1, Materials and  
690 Methods) and treatment initiated at the peak of the acute stage, day 14. (A-D) Ventral (V) and  
691 dorsal (D) images of representative individual mice. (A) Infected, non-treated. (B) Treated  
692 with 100 mg/kg benznidazole on days 14 – 33 post-infection, then immunosuppressed by 200  
693 mg/kg cyclophosphamide treatment on days 49, 53, and 57. (C) Treated and cured with 20  
694 mg/kg posaconazole (Noxafil formulation) on days 14 – 33, and immunosuppressed as above.  
695 (D) Treated with posaconazole (Noxafil formulation) on days 14 - 33, and  
696 immunosuppressed as above. 16 out of 19 posaconazole treated mice were assessed as non-  
697 cured. One mouse did not become infected and was excluded from the study. (E) *Ex vivo*  
698 imaging of organs and tissues obtained from mice on days 74 – 79, as indicated, following  
699 drug treatment and immunosuppression. Organs and tissues were arranged as in Fig. 1E (v).  
700 Heat-maps are on log<sub>10</sub> scales and indicate intensity of bioluminescence from low (blue) to  
701 high (red).

702

703

704

705

706

707

708

709

710

711

712

713 **FIG 7.** *Ex vivo* imaging of cyclophosphamide-induced parasite recrudescence following  
714 posaconazole treatment of mice in the acute and chronic stages of infection. (A) Mice in the  
715 acute stage of *T. cruzi* infection were treated with posaconazole for 20 days and then treated  
716 with cyclophosphamide (see legend to Fig. 6 for details). Images were taken 74 dpi. For  
717 comparison, the lower image shows parasite recrudescence following immunosuppression of  
718 a non-treated, chronically infected mouse (imaged 173 dpi). (B) *T. cruzi* infected mice,  
719 treated with posaconazole during the chronic stage of infection and then treated with  
720 cyclophosphamide (see legend to Fig. 1). Images taken 147 (upper) and 148 (lower) dpi. The  
721 schematic identifies the positions of organs (Gut Mes, gut mesentery tissue; OES,  
722 oesophagus; SKM, skeletal muscle; STM, stomach; VIS FAT, visceral fat/adipose tissue).  
723 The location of the visceral fat tissue is highlighted by an arrow. Heat-maps are on log<sub>10</sub>  
724 scales and indicate intensity of bioluminescence from low (blue) to high (red).

725

726

727

728

729

730

731

732

733

734

735

736

737

738 **Table 1.** Summary of drug efficacy against acute and chronic *Trypanosoma cruzi* infections  
739 inferred from bioluminescence. Data were collated from experiments illustrated in Fig. 1, 4  
740 and 6. Mice were designated as cured only when bioluminescence negative by both *in vivo*  
741 and *ex vivo* imaging following immunosuppression (Materials and Methods). In the  
742 posaconazole treatment, data from both formulations were pooled.

743

<b>Drug</b>	<b>Disease state</b>	<b>Treatment time</b>	<b>Daily dose</b>	<b>Number cured</b>
Benznidazole	chronic	20 days	100 mg/kg	5/5
Benznidazole	acute	20 days	100 mg/kg	5/5
Benznidazole	chronic	10 days	100 mg/kg	6/6
Benznidazole	chronic	5 days	100 mg/kg	6/6
Posaconazole	chronic	20 days	20 mg/kg	0/9
Posaconazole	acute	20 days	20 mg/kg	3/19

744

745

746

747

748

749

750

751

752

753

754

755

756

757

758

759

760

761

762

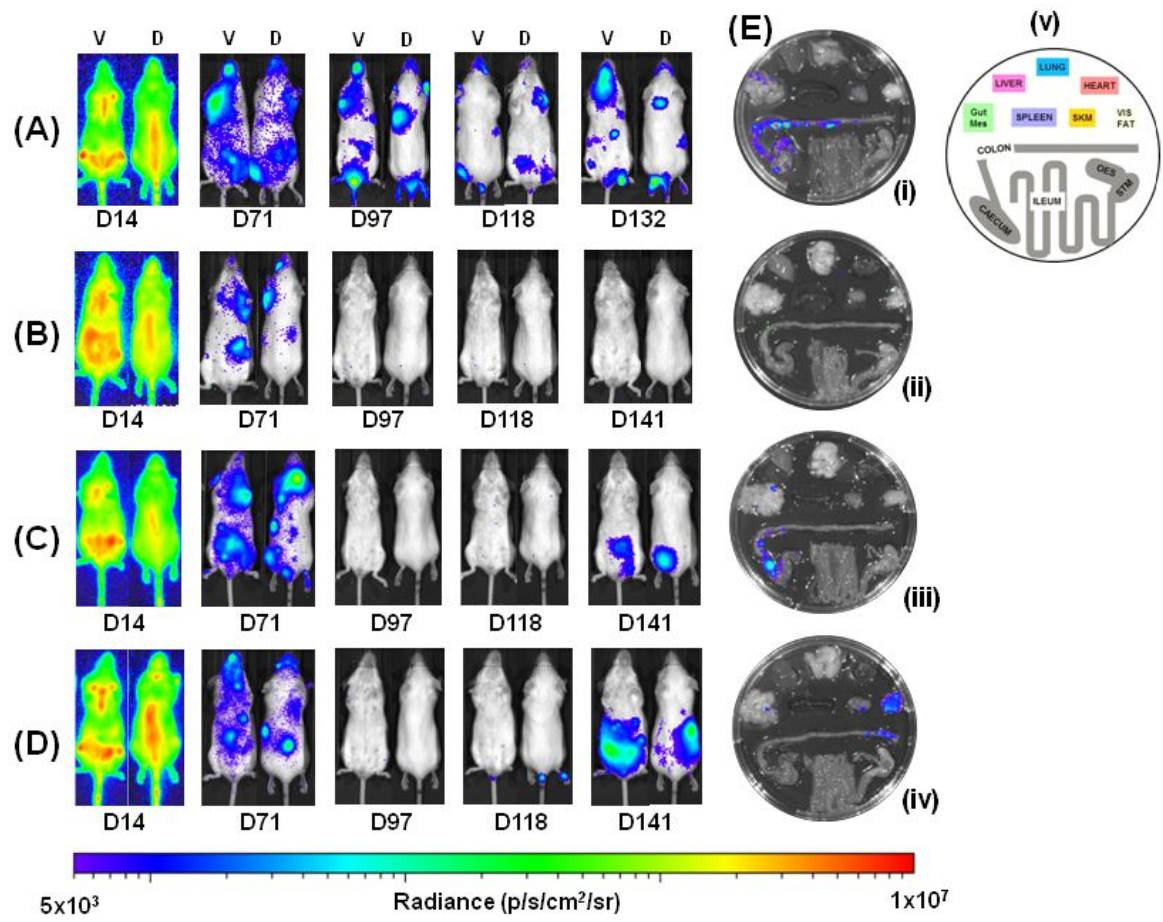


Fig. 1

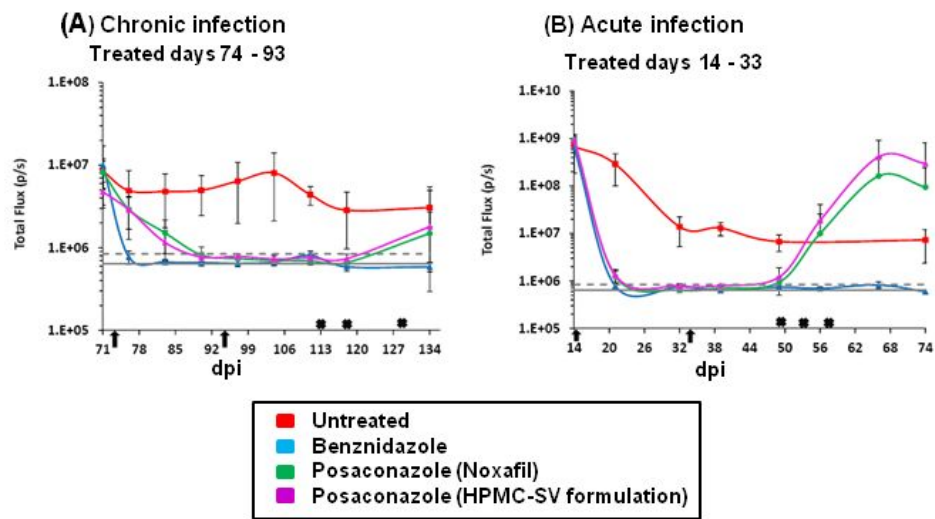


Fig. 2

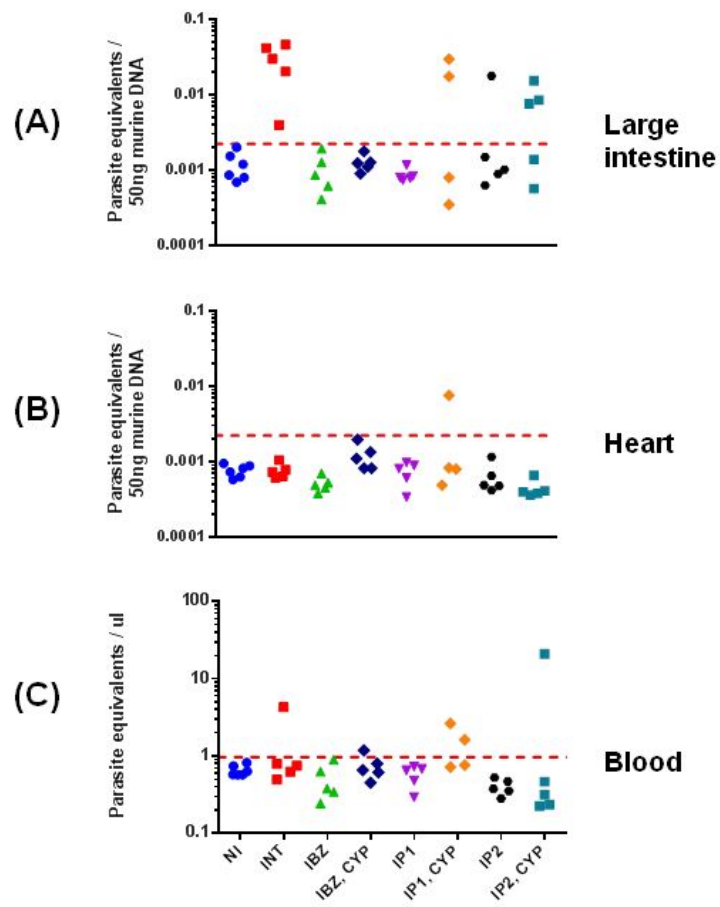


Fig. 3

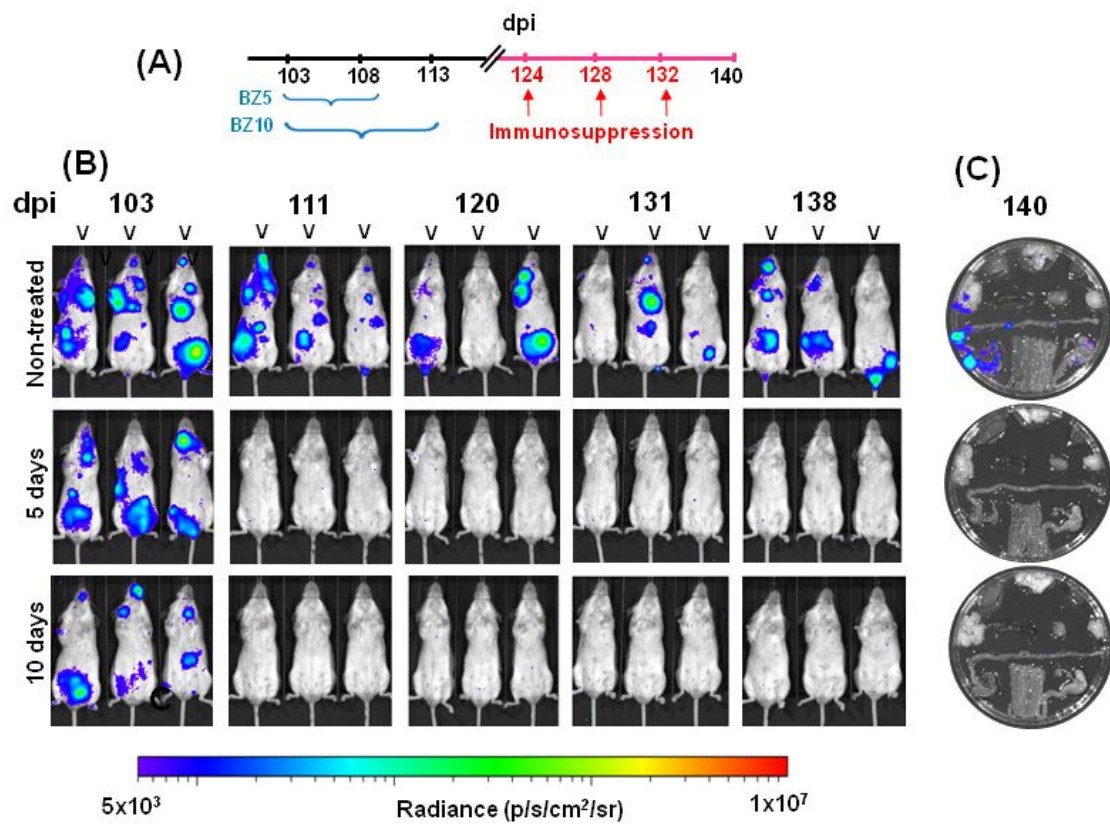


Fig. 4

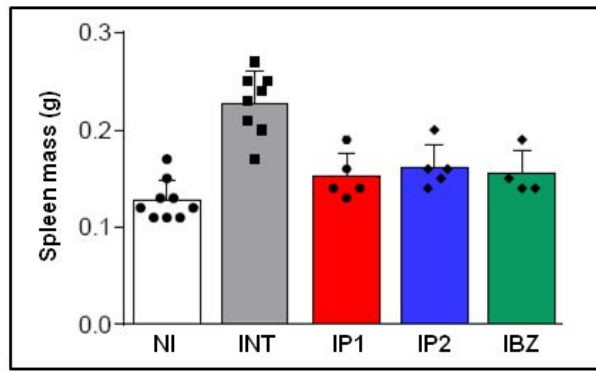


Fig. 5

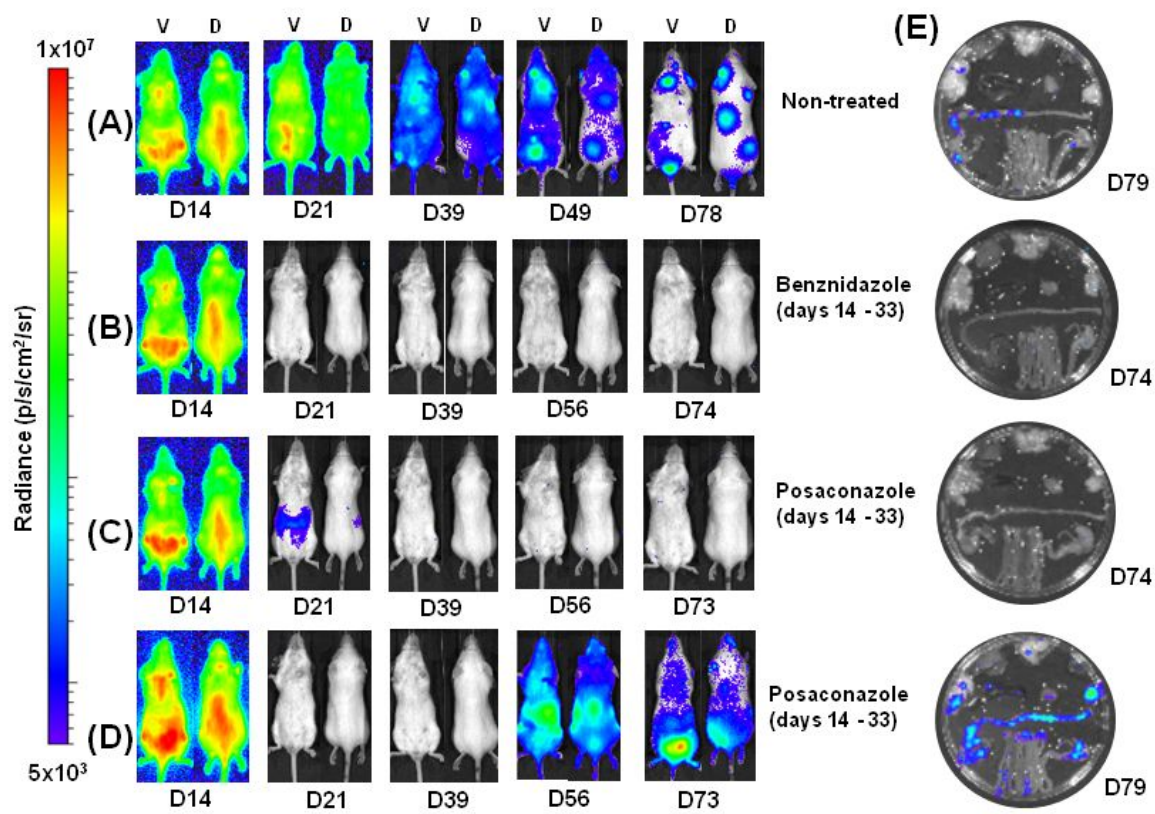


Fig. 6

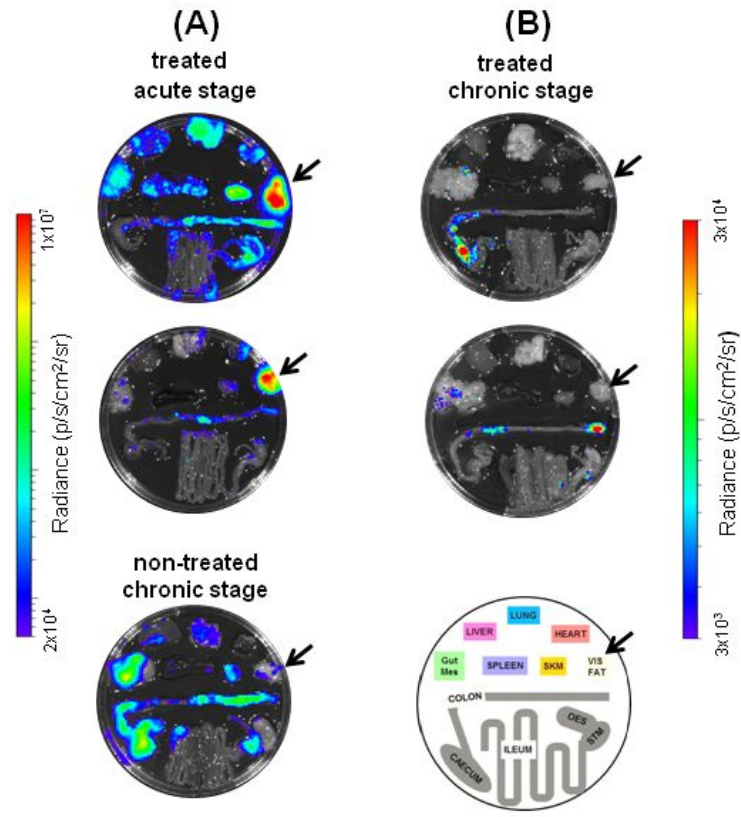


Fig. 7